

1 **Comprehensive two- dimensional liquid chromatography as a biomimetic screening platform for**
2 **pharmacokinetic profiling of compound libraries in early drug development.**

3
4 Giacomo Russo^{1,2}, Lucia Grumetto^{3,4}, Mathijs Baert¹, Frederic Lynen^{1*}

5
6 1. Separation Science Group, Department of Organic and Macromolecular Chemistry, Ghent
7 University, Krijgslaan 281, S4-bis, B-9000 Gent, Belgium

8 2. School of Applied Sciences, Sighthill Campus, Edinburgh Napier University, 9 Sighthill Ct, EH11
9 4BN Edinburgh, United Kingdom.

10 3. Department of Pharmacy, School of Medicine and Surgery, University of Naples Federico II, Via
11 D. Montesano, 49, I-80131 Naples, Italy.

12 4. Consorzio Interuniversitario INBB, Viale Medaglie d'Oro, 305, I-00136, Rome, Italy.

13 ** corresponding author*

14
15 To whom correspondence should be addressed:

16 Prof. Dr. Frederic Lynen

17 Separation Science Group

18 Department of Organic and Macromolecular Chemistry

19 Ghent University

20 Krijgslaan 281, S4-bis

21 B-9000 Gent, Belgium

22 Tel. +(32)9 264 96 02

23 Fax +(32)9 264 49 98

24 e-mail: frederic.lynen@ugent.be

25 **Comprehensive two- dimensional liquid chromatography as a biomimetic screening platform for**
26 **pharmacokinetic profiling of compound libraries in early drug development.**

27
28 Giacomo Russo^{1,2}, Lucia Grumetto^{3,4}, Mathijs Baert¹, Frederic Lynen^{1*}

29
30 1. Separation Science Group, Department of Organic and Macromolecular Chemistry, Ghent
31 University, Krijgslaan 281, S4-bis, B-9000 Gent, Belgium

32 2. School of Applied Sciences, Sighthill Campus, Edinburgh Napier University, 9 Sighthill Ct, EH11
33 4BN Edinburgh, United Kingdom.

34 3. Department of Pharmacy, School of Medicine and Surgery, University of Naples Federico II, Via
35 D. Montesano, 49, I-80131 Naples, Italy.

36 4. Consorzio Interuniversitario INBB, Viale Medaglie d'Oro, 305, I-00136, Rome, Italy.

37 * *corresponding author*

38

39 **Abstract**

40 A comprehensive two-dimensional liquid chromatography-based biomimetic platform (LCxLC) has
41 been developed and validated for drug diffusion studies. Human serum albumin and Immobilized
42 Artificial Membrane were thereby used in the first (¹D) and second (²D) separation dimension,
43 respectively. While the former was meant to emulate the blood, the latter was instead intended
44 to mimic the intestinal mucosa epithelium. Therefore, the experimental conditions, *i.e.* pH,
45 temperature and buffer composition, were modulated to reflect faithfully *in vivo* conditions. 30
46 compounds, whose effective intestinal permeability (P_{eff}) assayed *in situ* on humans by a validated
47 technique was known from the literature, were used as model drugs.

48 A good and orthogonal separation was achieved for the whole dataset, although for a better
49 distribution of the most polar compounds in the elution window a segmented gradient elution
50 program had to be employed. Interestingly, the passively uptaken compounds having the most
51 favorable P_{eff} , populated a specific area of the 2D plots, implying that the affinity for HSA and IAM
52 has to lie in specific ranges in order for a compound to be satisfactorily absorbed from the
53 intestinal lumen.

54 Although these results should be regarded as preliminary, this work paves an entirely new and
55 unprecedented way to profile pharmaceutically relevant compounds for their *in vivo* absorption
56 and distribution potential.

57

58 *Keywords:* Immobilized Artificial Membrane; Human Serum Albumin; effective intestinal
59 permeability; comprehensive two-dimensional liquid chromatography; ADMET profiling;
60 bioaffinity chromatography.

61

62

63

64

65

66

67

68

69

70

84 In brief, some drug products could be considered for biowaiver, *i.e.* approved by providing only
85 dissolution test outcomes rather than envisaging full bioequivalence studies on human subjects,
86 with the proviso that (a) these formulations are immediate-release (85% of the drug released
87 within 30 minutes) (b) the dose is fully soluble in water over a 1.0-7.5 pH range (c) the intestinal
88 absorption is almost quantitative (fraction absorbed >90%) [5]. While water solubility is fairly easy
89 to measure, permeability should be instead properly assayed to achieve correct BCS classification
90 [6]. For instance, the food and drug administration (FDA) currently accepts absorption data only if
91 intestinal uptake evidence is produced by human pharmacokinetic (PK) studies (mass balance or
92 absolute BA) or *in vivo* intestinal perfusion in human subjects [7]. Alternatively, *in vivo* or *in situ*
93 intestinal perfusion methods based on murine models, as well as models based on excised tissues
94 or cellular monolayers, can as well be used. However, these procedures must be properly
95 validated and even in that case their reliability is still regarded with extreme caution, as
96 interlaboratory variability of data based on cell protocols is generally high. Indeed, uptake studies
97 performed on such systems are claimed trustworthy only if the absorption is demonstrated to
98 occur exclusively by passive diffusion, *i.e.* without any involvement of ATP-operated protein
99 channels [7]. Consistently, the FDA encourages biowaiver applications providing intestinal
100 absorption outcomes from different methodologies and in case of conflicting information, human
101 data supersede *in vitro* or animal data.

102 The gold standard of permeability determinations has long been considered the intubation and
103 perfusion of a drug solution *in situ* in healthy human volunteers [2]. This approach (so called LOC-I-
104 GUT perfusion technique) has been used for over 50 years, and effective permeability (P_{eff}) values
105 determined by this method give the best indication as to whether a drug compound has a
106 sufficient potential for absorption. In brief, to allow the perfusion of a drug solution in a human, a
107 radiopaque multichannel perfusion tube is inserted through the mouth and positioned in a region

108 comprised between the proximal to mid-small intestine [8]. Once the tube is correctly placed, a
109 perfusion solution is continuously administered through one of the channels in the tube, and
110 subsequently collected from other channels. P_{eff} is determined by measuring the disappearance of
111 an API from the intestinal lumen by perfusion and is equal to:

$$112 \quad P_{eff} = \frac{-Q_{in} \cdot \ln\left(\frac{C_{out}}{C_{in}}\right)}{A} \quad \text{Eq. (1)}$$

113 where Q_{in} is the perfusate flow rate, C_{out} and C_{in} are the concentrations of API leaving and entering
114 the intestinal segment, and A is the surface area of the perfused intestinal segment, which is
115 assumed to be a smooth cylinder [8]. However, as human intestinal perfusion requires patients'
116 hospitalization and follow-up, this technique is time- and resource- consuming. Due to these
117 considerations, albeit valuable, human intestinal perfusion work is hardly performed.

118 Alternative methods, based on separation science, are increasingly gathering the attention of the
119 scientific community [9, 10]. These methods allow the introduction in the separation mode of
120 biological structures playing an essential role in drugs' absorption such as membrane
121 phospholipids and plasma proteins [11, 12]. The advantage lies in (a) a superior reproducibility of
122 the measurements as compared to data achieved by the culturing of suitable cell monolayers, *e.g.*
123 Caco-2 cells, (b) their greater speed as compared to screening methodologies implemented on
124 animal (human included) models and (c) the aspect that, being based on physico-chemical
125 parameters, they allow elucidation of molecular mechanisms.

126 Chiral protein-based stationary phases, such as those based on human serum albumin (HSA), are
127 commercially available and were successfully used for both chiral separation and plasma protein
128 binding assessment purposes in high performance liquid chromatography (HPLC) set-ups [13]. HSA
129 is indeed the most abundant plasma protein found in human blood. Produced by the liver, HSA
130 has a 35-50 g L⁻¹ reference blood concentration range and binds preferably acidic compounds [14].
131 Although HSA typically engages with analytes through non-specific hydrophobicity-driven

132 interactions, certain protein domains were demonstrated to be capable to recognize enantiomers
133 thanks to the presence of specific interaction sites. At least two major enantioselective sites, *i.e.*
134 Site I (binding warfarin) and Site II (binding diazepam), have been described on HSA [15].

135 Immobilized artificial membrane (IAM) are stationary phases based on phosphatidylcholine (PC)-
136 analogues covalently bound to a silica core exploited in reversed phase HPLC [16, 17]. They
137 represent a rather simplified model of complex lipoidal biological bilayers with the main
138 shortcomings being the monolayered nature of the membrane and the aspect that only one
139 phospholipid, *i.e.* PC, is represented. Nevertheless, IAM-HPLC was proved effective in predicting
140 the extent at which drugs cross biological membranes of strategic relevance in biopharmaceutics
141 such as the blood-brain barrier, the intestinal tract and the skin [18-25].

142 To the best of our knowledge, to date either IAM or HSA HPLC have been extensively and
143 successfully employed in only one-dimensional liquid chromatography approaches for the
144 characterization of pharmacokinetic and biodistribution properties of APIs. In recent years, the
145 need of separating and characterizing more and more complex samples has led to the
146 development of increasingly smaller particles and consequently of hardware capable of
147 withstanding comparatively higher operating pressure [26]. However, this trend seems to have
148 terminated in its natural evolution and chromatographers and separation scientists have focused
149 their attention on multidimensional liquid chromatographic approaches as more powerful
150 solutions to generate superior separation capacity [27].

151 In this work, a comprehensive two-dimensional platform has been for the first time developed in
152 fully biomimetic separation conditions and applied on 30 compounds whose intestinal effective
153 permeability was known from one single bibliographic source to exclude any interlaboratory
154 variability. The achieved separation has been eventually evaluated from both an analytical and a
155 biopharmaceutical perspective.

156

157

158 **2. Materials and Methods**

159

160 **2.1 Chemicals and reagents**

161

162 The solutes were obtained from Merck (Machelen, Belgium), TCI-Europe (Zwijndrecht, Belgium),
163 Thermofisher Acros Organics (Geel, Belgium) and Sanbio (Uden, The Netherlands) as listed in Table
164 1. Naproxen, (+)-warfarin and (-) warfarin were purchased from Merck. The purity of all the tested
165 solutes was equal to or higher than 98%. Water ($18.2 \text{ M}\Omega\cdot\text{cm}^{-1}$) was purified and deionized in
166 house via a Milli-Q plus instrument from Millipore (Bedford, New Hampshire, USA). Acetonitrile
167 and methanol used for the preparation of the eluents were HPLC grade and obtained from
168 Biosolve (Valkenswaard, The Netherlands). Potassium phosphate monobasic and ammonium
169 acetate were both from Sigma-Aldrich (Machelen, Belgium) and their purity was equal to and
170 higher than 99%.

171

172 **2.2 LC analytical columns**

173

174 The ¹D column was a Chiralpak HSA 150 x 2 mm i.d., 5 μm (Daicel, Raunheim, Germany) used with
175 a Chiralpak 10 x 4 mm guard cartridge inserted in a cartridge holder and a column coupler (both
176 for protein-based analytical columns), while the ²D column was a IAM.PC.DD2, 150 x 4.6 mm i.d.,
177 10 μm (Regis Technologies, Morton Grove, USA).

178

179 **2.3 2D LC system**

180

181 The ²D LC instrument was assembled from two Agilent 1100 systems (Agilent Technologies,
182 Waldbronn, Germany), interfaced via a 2-position/10-port switching valve with a microelectric
183 actuator (VICI, Houston, U.S.A., model C2H-2000EH). The ¹D separation was performed using an
184 1100 quaternary pump equipped with a 1100 degasser coupled to an external six-port injection
185 valve (Rheodyne, Alsbach, Germany). The temperature was controlled by an Agilent 1100 Series
186 Thermostatted Column Compartment. An 1100 variable wavelength detector (VWD) equipped
187 with a micro flow cell was used to monitor the ¹D separation. The ²D instrument consisted of an
188 1100 binary pump, 1100 degasser, and 1100 VWD equipped with a standard flow cell. All modules
189 were controlled using two Windows-based computers equipped with ChemStation software
190 (Agilent). The first was used to control the ¹D pump, ¹D detector, and ²D detector, and the second
191 computer was used to operate the ²D gradient on the ²D pump. The 10- port switching valve was
192 equipped with two 100 µL loops, and the modulation time was 2.0 min.

193

194 **2.4. Competitive binding and HSA Site I occupancy assessment**

195

196 *2.4.1 Mobile phases*

197

198 The HSA mobile phase was composed of a 100 mM ammonium acetate buffer solution (A) and a
199 75/25 (v/v) ammonium acetate buffer 100 mM pH 7/acetonitrile (B). The pH was adjusted at pH
200 7.0 by dropwise addition of ammonia. The mobile phase gradient applied on the IAM column in
201 the ²D comprised a 10 mM potassium phosphate monobasic (Sigma-Aldrich, Machelen, Belgium
202 purity ≥ 99%) buffer solution (A) and a 45/55 (v/v) 10 mM potassium dihydrogen

203 phosphate/acetonitrile (B) solution. The pH of this buffer was adjusted at pH 5.0 *via* dropwise
204 addition of hydrochloric acid.

205

206 *2.4.2 2D LC elution programs*

207

208 The ¹D separation was carried out at a 50 $\mu\text{L min}^{-1}$ flow rate and under controlled temperature (30
209 °C) by using a linear gradient elution program set as follows: 0 min: 0% B₁; 10 min: 0% B₁; 20 min:
210 40% B₁; 40 min: 50% B₁; 60 min: 50% B₁; 100 min: 85% B₁; 180 min: 100% B₁; 200 min: 100% B₁.

211 The ²D separation was carried out at 5.0 mL min^{-1} and at room temperature, *i.e.* 25 ± 2 °C, by using
212 a linear gradient elution program set as follows: 0 min: 25% B₂; 1.50 min: 100% B₂; 1.51 min: 25%
213 B₂; 2 min: 25% B₂.

214

215 **2.5 Bioaffinity measurements**

216

217 *2.5.1 Mobile phases*

218

219 The HSA mobile phases consisted of a 100 mM potassium phosphate monobasic buffer solution
220 (A) and a 75/25 (v/v) a 100 mM potassium dihydrogen phosphate/2-propanol (HPLC grade,
221 Biosolve, Valkenswaard, The Netherlands) solution (B). To mimic the blood compartment, the pH
222 was adjusted with hydrochloric acid and the aqueous solution had a pH value of 7.00 ± 0.05 . The
223 IAM mobile phases were the same as that used for the calibration and described in 2.4.1.

224

225 *2.5.2 2D LC elution programs*

226

227 Two different separation methods were developed. In both cases, the ¹D separation was carried
228 out at a 50 $\mu\text{L min}^{-1}$ flow rate and under controlled temperature (30 °C) by using a linear gradient
229 elution program set as follows: 0 min: 0% B₁; 20 min: 0% B₁; 120 min: 100% B₁; 200 min: 100% B₁.
230 In both analytical methods, the ²D separation was carried out at 5.0 mL min⁻¹ and at room
231 temperature, *i.e.* 25 \pm 2 °C. However, in a first method a fixed linear gradient ²D elution program
232 was set as follows: 0 min: 25% B₂; 1.50 min: 100% B₂; 1.51 min: 25% B₂; 2 min: 25% B₂, whereas in
233 a second method a mixed gradient elution method was used. Therefore, from 0 to 36 min the
234 program was set as follows: 0 min: 0% B₂; 1.50 min: 55% B₂; 1.51 min: 0% B₂; 2 min: 0% B₂ and
235 from 36 to 200 min the composition of the eluents was changed as follows: 0 min: 25% B₂; 1.50
236 min: 100% B₂; 1.51 min: 25% B₂; 2 min: 25% B₂.

237 After preparation, all the mobile phases were *vacuum*- filtered through 0.20 μm nylon membranes
238 (Grace, Lokeren, Belgium) and degassed in an ultrasonic cleaner (Branson 2510, Frequency: 40
239 kHz, Branson Ultrasonics, Danbury, USA) for 20 minutes before use.

240

241 **2.6 Sample preparation**

242

243 Stock solutions of all drugs were prepared by dissolving 10 mg of each solute in 2 mL of methanol
244 and kept at -4 °C, except for cyclosporin A which was dissolved in DMSO and stored -20°C.
245 Working solutions were freshly prepared at the beginning of each day by dilution of the stock
246 solutions to 50 $\mu\text{g mL}^{-1}$ with the starting mobile phase for all the analytes. Nifedipine samples and
247 nifedipine-containing mixtures were wrapped in aluminium foil before feeding the autosampler to
248 protect this chemical from photodegradation.

249

250 **2.7 LC experimental conditions**

251

252 The injection volume for each analysis was 10 μ L. The calibration was recorded at 254 nm UV
253 wavelength whereas the bioaffinity measurements were monitored at 220 nm UV wavelength.

254

255 **2.8 Postprocessing**

256

257 Raw data were exported as comma-separated values and converted to a data matrix in GC image
258 R2.5 software (GCimage, Lincoln, U.S.A.). From these matrices, contour plots and 3D scatterplots
259 were generated by using OriginPro 8.5 (OriginLab Corporation, Northampton, U.S.A.). The
260 chromatographic retention factors of each analyte were calculated by using Eq. (S1).

261

262 **2.9 Data sources**

263

264 For the scatterplots, *n*-octanol/water lipophilicity values either of the neutral forms of the
265 analytes, *i.e.* $\log P^N$, and of the mixtures present in solution at pH 7.4, *i.e.* $\log D^{7.4}$ were collected
266 from the scientific literature [28, 29] (except for creatinine, fexofenadine, whose $\log P^N$ and \log
267 $D^{7.4}$ values were calculated and for cyclosporin A, lisinopril, losartan, L-phenylalanine and
268 valacyclovir, whose $\log D^{7.4}$ but not $\log P^N$ values were calculated), whilst all *n*-octanol/water the
269 mixtures present in solution at pH 5.0, *i.e.* $\log D^{5.0}$, were calculated, except for acetaminophen, (+)-
270 griseofulvin and nifedipine, which do not support any ionizable moiety and, as a consequence of
271 that, their $\log P^N$ values were assumed as reasonable estimates of their $\log D$ values at both pH
272 values. The calculation of lipophilicity values was accomplished by the software Marvin Sketch
273 17.1.23.0 on a Windows-based quad-core PC [30]. Effective human jejunum permeability (P_{eff})

274 data were taken from [31, 32]. When more than one P_{eff} value was reported, an average was
275 considered.

276

277

278 **3.0 Results and Discussions**

279

280 **3.1 Method development**

281

282 Protein-based liquid chromatographic stationary phases are generally used for bioaffinity
283 chromatography. Therefore, method development conducted on such phases, even in 1D, poses
284 several constraints, regardless of these being exploited for protein binding assessment or for mere
285 chiral separation purposes. Indeed, deliberate deviations from the recommended pH range (5.0-
286 7.0), temperature (20-30 °C), operating pressure (lower than 150 bar), buffer concentration (up to
287 100 mM) and types (ammonium acetate or phosphates), organic modifier ratio (0-15% v/v for
288 analysis, max 25% for decontamination) and type (2-propanol or in general alcohols preferred) can
289 lead to significant reduction of column lifetime and loss of reproducibility [33]. The manufacturer
290 suggests the usage of charged additives such as N,N-dimethyloctyl amine (DMOA), trifluoroacetic
291 acid (TFA), octanoic acid (OA), heptafluorobutyric acid to be added to the mobile phases at a
292 concentration not higher than 2, 10, and 5 mM, respectively to modulate retention and
293 enantioselectivity [33].

294 However, in our study this was not an option since, as the manufacturer acknowledges, these
295 additives have such a strong affinity for the matrix that they end up being very difficult, if not
296 impossible, to remove quantitatively. Consistently, the manufacturer suggests that if the

297 separation scientist wishes to include such cationic or anionic additives as part of method
298 development then “the column should be dedicated for the purpose”.

299 This work is aimed at prospecting the selectivity of two different stationary phases embedding
300 biological structures that are crucial for drug absorption (IAM) and distribution (HSA) in a 2D LC
301 setting. For this reason, in the method development we were concerned not only on allowing a
302 satisfactory separation of the analytes under consideration, but also the on ensuring that the
303 analyses were realized in conditions able to mirror as closely as possible the biological
304 compartment in which absorption and distribution take place. To fulfil this goal, we worked to
305 assure that the affinity indexes achieved from the biomimetic measurements had solid physico-
306 chemical meaning and accuracy and that these both were retained over time.

307 Consistently, the utmost care was put in preserving the performance of the biomimetic LC
308 columns over time. This was achieved by optimizing on one hand the capability of the separation
309 process to account for the highly specific recognition forces and molecular interactions that occur
310 *in vivo*. On the other hand, we compromised for a longer column lifetime and no deviation from
311 the ideal chromatographic behaviour that these phases feature. For instance, although some
312 authors [9] conducted plasma protein binding measurements on HSA column applying conditions
313 differing from those recommended by the manufacturer (high flow rates, *i.e.* 1.8 mL min⁻¹ on a 50
314 x 3 mm, mobile phase at pH 7.4, 30% (v/v) 2-propanol), we preferred to strictly adhere to these,
315 even if this may effect in longer run times. This is because we designed this biomimetic platform
316 with a potential to be exploited in drug development programs in which large compound libraries
317 are assayed daily and data reproducibility is crucial. Consistently, although the pH of the blood
318 compartment in physiological condition is 7.4, the ¹D mobile phase pH was set to 7. This is
319 motivated by the instance that the HSA column should not be used at a pH above 7.0 according to
320 the column manufacturer [33]. A pH 5 was chosen to mimic that of the duodenum and the small

321 intestine. These are the regions of the gastrointestinal tract that are mainly involved in drugs'
322 absorption, thanks to the very large surface area (*ca.* 80 cm² cm⁻¹) that they provide along with
323 their typically long transit time (>3 h) [34].

324

325 The results of a performance check are described in section S1.0 of supporting information
326 whereby representative chromatograms are shown in Figure S1 and S2 along with the
327 experimentally determined chromatographic retention coefficients and resolution values which
328 are listed in Table S1. The HSA column features enhanced affinity for neutral and especially acidic
329 compounds and the capability of the stationary phase to resolve a (±)-warfarin racemate was
330 assumed as an indication of Site I being intact. This assures that the HSA affinity indexes depict not
331 only unspecific – generally lipophilicity- driven – interactions, but also highly specific recognition
332 forces, which are responsible of enantioselectivity. On the contrary, the IAM phase exhibits
333 superior retention of cations, whereas acids are on average less retained than neutral compound
334 having same lipophilicity values in agreement with Avdeef's "pH piston hypothesis" [35].
335 According to this, cations would be favored with regards to neutral compounds of same
336 lipophilicity in the interaction with IAM.PC phases as its negatively charged phosphate moieties
337 locate more internally as compared to the positively charged amino groups. This allows bases to
338 have a deeper and more productive interaction of electrostatic nature and to better
339 accommodate their apolar moieties in the hydrophobic tails of the lipid network, especially as
340 compared to acidic solutes. Therefore, in our design we chose to conduct the separation in ¹D on
341 the HSA phase and in ²D on the IAM phase, to allow satisfactorily orthogonality, which implies that
342 the separation mechanisms used in each dimension are independent of each other [36].

343 First of all, we had to verify that the given (re-)equilibration volume in the ²D separation was
344 suitable to achieve reproducibility in both retention time and chromatographic peak profile. To

345 find out this the separation was studied in ¹D and the same chromatographic conditions described
346 in 2.4.2 were applied, but the flow rate was halved and consequently broadened the separation
347 window by two times. This was done to allow assessment of even small discrepancies in the
348 chromatographic signals by visual inspection. The experimental procedure is properly detailed in
349 2.0 of the supporting information.

350 In brief, both the conditions detailed in 2.4.2 and that discussed in 2.5.2 for the first 36 minutes of
351 the mixed gradient elution program were applied. For the sake of conciseness, only the
352 chromatograms achieved by applying the former are discussed, but the results obtained were
353 highly comparable. The column was equilibrated by flushing 50.0 mL, *i.e.* 20 column volumes, at
354 constant flow rate, *i.e.* 2.5 mL min⁻¹ of the starting mobile phase and then three different samples
355 (carbamazepine, desipramine, naproxen) and one sample mixture (acetaminophen, antipyrine,
356 carbamazepine and naproxen) were injected for four consecutive times. Figure 1 shows excellent
357 reproducibility of the measurements over the four runs and demonstrate that only 2.5 mL, *i.e.*
358 only one column volume, is sufficient to allow complete column re-equilibration. This most
359 probably takes place because the overall variation in the acetonitrile concentration is only 30%
360 (v/v) in both the elution programs. However, it is worth noting that while conventional LC
361 protocols recommend to equilibrate columns by flushing from 10 to 20 column volumes it is
362 common practice in LCxLC to significantly reduce this [37]. Lower equilibration volumes (0.5-1.0-
363 1.5 and 2.0 mL were tested) led to unreproducible results, with not overlappable signals and
364 compromised peak symmetry (data not shown). Consistently, Venter and co-workers used only 1.6
365 column volumes for re-equilibration but the gradients applied spanned from totally aqueous (with
366 0.1% v/v formic acid) to 100% acetonitrile [38].

367 Despite the potential of stationary phase components such as silica to engage nonspecific
368 secondary interactions, most reports [39] indicate that immobilized HSA conserves the binding

369 properties of the protein in solution, allowing fast and reliable analyses of binding interactions.
370 However, a further complication lies in the aspect that one or more drug molecules can in
371 principle compete for the same binding site, producing potentially diverse retention times when a
372 compound is analysed alone or in mixture with one or more competitive displacers [40]. Although
373 partial and allosteric competitions have been studied with HSA HPLC, a complete displacement has
374 never been reported [39]. However, a noticeable example of this is the diazepam/ibuprofen co-
375 binding [41]. To avoid any possible co-binding, we took the following arrangements: all the solutes
376 were injected individually and no retention time shifts were recorded when they were instead
377 injected in the same mixture and a competitive binding and HSA Site I occupancy assessment with
378 10 model drugs and an allosteric binder, *i.e.* (\pm)-warfarin, was run before each biomimetic
379 measurement to investigate about possible competitive binding with Site I of the HSA and rate of
380 occupancy of this enantioselective site.

381

382 **3.2 Competitive binding and HSA Site I occupancy assessment**

383

384 The results of this assessment are shown in Figure 2. Clearly, except for the most polar
385 compounds, *i.e.* acetaminophen and antipyrine, which overlap, a good orthogonal separation is
386 achieved for all the assayed solutes. Evidently, (+)-warfarin and (-)-warfarin display a different
387 interaction toward the HSA phase, being the former less retained than the latter. Analogously,
388 another acidic racemate, *i.e.* (\pm)-ketoprofen, is resolved in its enantiomers. These results go well
389 with the studies conducted by Zou and co-workers [42], which determined the stereoselective
390 binding of warfarin and ketoprofen to HSA by both microdialysis and 1D HSA HPLC. The authors
391 concluded that the S-enantiomers ((+)-ketoprofen and (-)-warfarin) bind to the HSA more strongly
392 than (R)-enantiomers to HSA and that HSA exhibit stronger stereoselectivity to warfarin than to

393 ketoprofen racemates [42]. This is in full agreement with our findings as the resolution of the (\pm)-
394 warfarin is evidently superior to that of (\pm)-ketoprofen signals, as can be inferred from Figure 2.
395 Consistently, the IAM phase exploited in ²D did not allow any chiral separation and both
396 enantiomers exhibited same IAM affinity. Although IAM.PC phases do feature an asymmetric
397 carbon atom in their structure, they have never been reported to act as chiral selectors [16].

398

399 **3.3 2D LC bioaffinity experiments**

400

401 The first 2D LC bioaffinity experiment is visualized in Figure 3. While no refocusing issues can be
402 observed, the applied chromatographic conditions in both dimensions evidently allowed poor
403 separation of roughly a third of the dataset (compounds 1-10). These are extremely polar
404 compounds ($-4.30 \leq \log P^N \leq 0.53$), whose interaction with both stationary phases is rather limited.
405 The least retained compound on both dimensions was enalaprilat ($\log k^{HSA} = -0.886$ and $\log k^{IAM} = -$
406 2.332), the compounds exhibiting the strongest affinity were (+)-ketoprofen on the HSA ($\log k^{HSA} =$
407 1.246) and desipramine on the IAM ($\log k^{IAM} = 0.653$) phases. This is consistent with previous
408 studies regarding both the selectivity of the IAM phase [43] and that of HSA [44]. Three are indeed
409 the most lipophilic bases included in the dataset, *i.e.* desipramine ($pK_a = 10.40$), propranolol (pK_a
410 $= 9.45$) and verapamil ($pK_a = 8.92$)[45]. Among these, desipramine is the one featuring the highest
411 $[\text{cationic specie}]/[\text{neutral specie}]$ ratio at pH 5, and, in agreement with the “pH piston hypothesis”,
412 is the one having the strongest affinity with the IAM phase. Two are instead the acids
413 characterized by highest lipophilicity, *i.e.* fluvastatine ($pK_a = 5.50$ [46]) and ketoprofen ($pK_a =$
414 4.45 [45]). Again, between these, the analyte with a greater dissociation constant was retained for
415 a longer time, thus confirming the affinity of the HSA phase for acidic solutes. Clearly, no
416 breakthrough or peak refocusing issues are observable. As expected, chiral separation occurred

417 preferably for acidic racemates, *i.e.* (\pm)-fexofenadine, (\pm)-fluvastatin and (\pm)-ketoprofen, for which
418 anyhow the HSA matrix is known to have stronger affinity. However, although no chiral resolution
419 was achieved for the basic racemates (\pm)-atenolol, (\pm)-metoprolol and (\pm)-propranolol, the (\pm)-
420 verapamil racemate was instead enantioselectively retained to some extent. Interestingly, even if
421 a fluvastatin/salicylic acid competitive binding to the HSA has been reported by Tse *et al.* [47], no
422 variation in the retention factors was recorded when these compounds were individually
423 measured. Furthermore, Jattinagoudar and co-workers claimed that according to spectroscopy
424 and molecular docking-based studies they carried out [48], the secondary structure of serum
425 albumin was changed in the presence of fexofenadine. In our experiments again no variation in
426 the chromatographic retention coefficient was appreciated, therefore if any structural
427 rearrangement took place, this had apparently a negligible influence on the bioaffinity
428 measurements. Indeed, the authors studied in interaction of fexofenadine with bovine serum
429 albumin (BSA) and not with HSA. Even though these two proteins share 76% sequence homology,
430 they however differ due to the presence of two tryptophan residues in BSA, with Trp-213 located
431 within a hydrophobic binding pocket in the subdomain IIA, and Trp-134 located on the surface of
432 the albumin molecule in subdomain IB [49]. Moreover, Jattinagoudar and co-workers conducted
433 fluorescence spectroscopy binding measurements by using relatively high fexofenadine levels, *i.e.*
434 5-45 μ M, to react with 2.5 μ M BSA [48]. This is (at least) 50 times higher than the concentrations
435 applied in HSA based HPLC.

436 As said, although a good and orthogonal separation was achieved for most of the assayed
437 compounds, this method failed in discriminating the most polar molecules. Conceivably, these
438 feature remarkably diverse P_{eff} values, consequently we decided to apply a segmented gradient
439 elution program in 2 D with the aim of broadening the separation window of the compounds
440 elution within the first 36 minutes.

441 The result of this further method development are shown in Figure 4. Evidently, the compounds
442 eluting within the first 36 minutes are much better distributed than before over the separation
443 space. Again a part from cyclosporine A, whose peak shape suffers from some fronting, the
444 majority of analytical signals have good peak shape, with carbamazepine, hydrochlorothiazide and
445 losartan featuring excellent symmetry. An inversion in the elution order is seen for antipyrine and
446 atenolol (compound 10 and 11), being the latter more retained in eluents richer in aqueous buffer.
447 Although this circumstance might be unexpected when LC is exploited on electrically neutral
448 stationary phases, this is instead reasonable when we consider that IAM phases are instead
449 electrically charged and exhibit preferential affinity for cations [18]. Both antipyrine and atenolol
450 are bases, however the first ($pK_a = 6.8$ [29]) is much weaker than the second ($pK_a = 9.6$ [29]).
451 Indeed, ionization is enhanced in fully aqueous phases as the addition of an organic modifier
452 lowers the dielectric constant of the medium. A possible explanation of this chromatographic
453 behaviour is that in pure aqueous eluent atenolol dissociates into its ions to a greater extent than
454 antipyrine, and its cations are more abundant at the experimental pH, *i.e.* 5.0, than its neutral
455 microspecies. However, when the starting mobile phase features already 25% (v/v), ionization
456 might occur to a lower extent and the contribution electrostatic and hydrophobic forces in the
457 whole separation mode is plausibly unbalanced slightly in favour of the latter. With this regards,
458 *n*-octanol/water lipophilicity of the neutral species of antipyrine ($\log P^N$) and of the distributions at
459 both pH 5.0 and 7.4 ($\log D^{5.0}$ and $\log D^{7.4}$) is greater for antipyrine than for atenolol.

460

461 **3.4 Biopharmaceutical implications**

462

463 So far, we have discussed the separation only from an analytical point of view, however much
464 attention has been paid in developing an analytical method that allowed the affinity index to

465 retain relevance also from a biopharmaceutical perspective. From Figure 5, it is evident that all the
466 compounds located in the same area (blue frame) have intestinal effective permeability higher
467 than $1 * 10^{-4} \text{ cm} * \text{s}^{-1}$, except for furosemide and (\pm)-fexofenadine, behaving as outliers. Actually,
468 furosemide was reported to be a substrate of a saturable active efflux transport system [50].
469 Consistently, the basolateral-apical apparent permeability of (\pm)-fexofenadine, estimated in Caco-2
470 monolayers, markedly reduced in the presence of increasing concentration of P-glycoprotein
471 inhibitors, suggesting that this efflux protein carrier is the main transport route for this
472 therapeutic [51]. The active uptake of xenobiotics requires ATP hydrolysis and occurs via specific
473 recognition of structural motifs that both the exploited separation modes cannot possibly depict.
474 However, it is relevant that all the compounds having intestinal absorption greater than a
475 threshold – except the two analytes above discussed – populate a specific region of the 2D plot.
476 We are aware that the size of the dataset may be relatively limited, however as already
477 highlighted in the introduction, these intestinal effective permeability experiments are hardly
478 performed due to ethical reasons and the criticism these human testing methodologies are
479 increasingly facing from the general public. Additionally, pooling biological activity data from
480 different sources might then transpire in a misleading exercise in the light of the aspect that
481 significant interlaboratory variability (sometimes even higher than 80%) has occasionally been
482 reported [52]. For this reason, we decided to select biological activity data from a single
483 bibliographic source. Moreover, one of the advantages of this screening platform is that the
484 results can be evaluated by simple visual inspection, while statistical modelling often requires
485 technical expertise and a sound background to be properly assessed.

486 However, some conventional modelling by calculating the affinity indexes on each dimension by
487 using Eq. (2) was still envisaged. We took into account the separation displayed in Figure 3 and
488 conducted by applying the conditions detailed in 2.5 because it is necessary that the bioaffinity

489 indexes are achieved in the same thermodynamic conditions to allow fair comparison. The affinity
490 data in each dimension, along with $\log P^N$, $\log D^{7.4}$, $\log D^{5.0}$, P_{eff} values and supplier are reported
491 in Table 1. Chemical structures are instead reported in Table S2. Interestingly, when the
492 partitioning values were plotted against biological data, no significant relationship was achieved in
493 all cases (Figure 6).

494 However, 3D scatterplots studying both HSA and IAM bioaffinity vs “classical” *n*-octanol/water
495 partition coefficients of the neutral species and of the neutral/ionized distribution both at blood,
496 *i.e.* 7.4, and at duodenum pH, *i.e.* 5.0 were then generated. These 3D scatterplots are represented
497 in Figure 7 and (B) and (C) could be considered as a simulation a 3D LC experiments in in which the
498 3D is exploited on a neutral hydrophobic phase, such as C18 or C8, and the aqueous eluent are
499 buffered at pH 7.4 and 5.0 respectively. In fact, retention on stationary phases based on
500 hydrocarbons has been proved to be driven by the lipophilicity of the distribution coefficients at
501 the experimental pH, although some secondary interactions can take place due to the free silanol
502 groups [53]. A further complication is that the *in vivo* intestinal mucosa features various degrees of
503 leakiness as a consequence of the different expression of tight junctions and this may allow some
504 paracellular passage. Pearce *et al.* demonstrated that the expression of certain tight junction
505 proteins varied with cell type, with occludin and tricellulin levels being high in both intestinal stem
506 cells (ISCs) and Paneth cells, and claudin-1, -2, and -7 expression being enhanced in Paneth cells,
507 ISCs, and enterocytes, respectively [54]. The paracellular passage pathway is likely for small
508 hydrophilic molecules, having sizes compact enough to slip through the cell-to-cell gaps. To
509 distinguish any possible involvement of paracellular passage, we deliberately split our dataset in
510 two subsets: compounds having mass weight (MW) inferior than 200 Da, for which a relevant
511 contribution of paracellular passage can be reasonably hypothesized, and analytes heavier than
512 200 Da, for which a pure transcellular migration is instead highly likely. Recent scientific reports

513 [55] suggest that molecular size and O plus N atom count and OH plus NH count of newly designed
514 drugs are steadily but constantly increasing, while molecular lipophilicity has remained relatively
515 unchanged. Therefore, since it might be challenging for pharma chemists dealing with rational
516 drug design to comply to a 200 Da MW constrain, predicting passive transcellular permeability is
517 much more valuable, especially if we consider that there might be a huge variation in the degree
518 of leakiness of intestinal cells among individuals. While plots (B) and (C) show a quite
519 homogeneous distribution of the subsets, interestingly most of the compounds having fair and
520 good effective intestinal permeability populate a specific area of plot (A), displayed in a red
521 square, with the exception of one datapoint, *i.e.* furosemide. The characteristics of this analytes
522 have already been discussed above.

523 Although further studies should be undertaken, these results seem extremely relevant and might
524 assist – alone or in combination with other methodologies – pharmaceutical chemists in screening
525 therapeutics for their intestinal absorption potential without sacrificing/distressing animals and/or
526 running complex and sometime resource-intensive statistical modelling.

527

528

529 **4.0 Concluding remarks**

530

531 A 2D comprehensive LC-based biomimetic platform has been for the first time developed and
532 validated as a screening tool for drug diffusion studies. The separation modes were based on
533 biological structures that are crucial for both drug absorption and distribution processes.
534 Specifically, a stationary phase embedding HSA, the most abundant plasma protein in humans,
535 was exploited in ¹D. An IAM phase, aimed at mimicking the lipoidal composition of plasma
536 membranes, was instead operated in ²D.

537 This set-up allowed a good and orthogonal separation of 30 model drugs, whose P_{eff} , assayed on
538 humans, was known from a single bibliographic source. Moreover, if we except two compounds
539 whose uptake is protein carrier- mediated, all the compounds populating the same area of the 2D
540 plots have P_{eff} greater than than $1 * 10^{-4} \text{ cm} * \text{s}^{-1}$. This implies that in order for a drug to be
541 successfully up taken, its affinity for these crucial biostructures has to lie in specific affinity ranges.
542 In addition, these bioaffinities were also studied vs classical *n*-octanol/water partitioning data and
543 visualized in 3D scatterplots. When the logarithm of the *n*-octanol/water partition coefficient of
544 the neutral species is plotted on the z axis (and HSA and IAM values on the x and y axis), again the
545 solutes having favourable P_{eff} and – for which an involvement of any paracellular passage
546 contribution is rationally unlikely – concentrate in the same region of the plots.
547 We acknowledge that these must be seen as preliminary results and further studies are needed to
548 further confirm this evidence. However, we also believe this design paves an entirely new way to
549 profile pharmaceutically relevant compounds for their *in vivo* absorption and distribution
550 potential.

551

552 **Acknowledgements**

553 G.R. acknowledges the Excellence of Science grant (30897864) of the FWO-FNRS for funding part
554 of this research.

555 **Table 1**

Compound	log k ^{HSA}	log k ^{IAM}	log P ^N	log D ^{7.4}	clog D ^{5.0} [30]	P _{eff} [31] (10 ⁻⁴ cm · s ⁻¹)	Supplier
acetaminophen	-0.221	-1.487	0.34[28]	0.34[28]	0.34[29]	1.76	Merck
amiloride	0.034	-0.320	-0.26[28]	-1.53[28]	-0.12	1.63	TCI
antipyrine	0.000	-0.403	0.56[28]	0.26[28]	1.61	4.45	TCI
(±)-atenolol	-0.221	0.294	0.22[28]	-2.01[28]	-3.31	0.21	Merck
carbamazepine	0.833	0.204	2.45[28]	2.45[28]	3.22	4.30	Merck
cimetidine	0.000	0.226	0.48[28]	0.34[28]	-1.27	0.44	Merck
creatinine	-0.167	-0.934	0.54[30]	0.53[30]	-0.05	0.30	Merck
cyclosporin A	0.415	0.632	1.40[29]	3.38[30]	3.38	1.63	TCI
desipramine	0.914	0.653	3.79[28]	1.38[28]	0.05	4.45	Merck
enalapril	-0.221	-1.218	0.16[28]	-1.75[28]	0.38	1.57	TCI
enalaprilat	-0.886	-2.332	-0.13[28]	-2.74[28]	-2.27	0.20	Sanbio
(+)-fexofenadine	1.108	0.184	5.68[30]	2.48[30]	2.45	0.47	Sanbio
(-)-fexofenadine	1.057						
(+)-fluvastatin	1.165	0.219	4.17[28]	1.14[28]	3.27	2.38	Sanbio
(-)-fluvastatin	1.128						
furosemide	1.094	0.002	2.56[28]	-0.24[28]	0.84	0.25	Acros
(+)-griseofulvin	0.893	0.331	2.20[28]	2.20[28]	2.20[29]	1.14	Acros
hydrochlorothiazide	0.532	0.043	-0.03[28]	-0.18[28]	-0.16	0.12	TCI
(+)-ketoprofen	1.246	0.145	3.16[28]	-0.11[28]	2.31	8.45	Merck
(-)-ketoprofen	1.226						
lisinopril	-0.301	-1.218	-1.01[29]	-4.30[30]	-4.25	0.33	Sanbio
losartan	1.017	0.422	1.19[29]	4.03[30]	5.24	1.14	Sanbio
L-phenylalanine	-0.398	-1.487	-1.38[29]	-1.67[30]	-1.67	4.07	Merck
(±)-metoprolol	0.000	0.380	1.95[28]	-0.24[28]	-2.08	1.16	Merck
nifedipine	0.881	0.555	3.17[28]	3.17[28]	3.17[29]	4.40[32]	Sanbio
piroxicam	1.153	0.087	1.98[28]	0.00[28]	0.56	7.06	Sanbio
(±)-propranolol	0.764	0.596	3.48[28]	1.41[28]	-1.07	2.82	Merck
ranitidine	0.205	0.373	0.45[28]	-0.53[28]	-1.87	0.37	Merck
salicylic acid	1.000	-0.485	2.19[28]	-1.68[28]	-0.27	2.67	Merck
terbutaline	0.069	-0.699	-0.08[28]	-1.35[28]	-2.40	0.30	Merck
valacyclovir	-0.699	-1.487	-0.30[29]	-1.26[30]	-3.35	1.66	Sanbio
(+)-verapamil	0.820	0.342	4.33[28]	2.51[28]	0.79	6.18	Merck
(-)-verapamil	0.858					6.21	

556

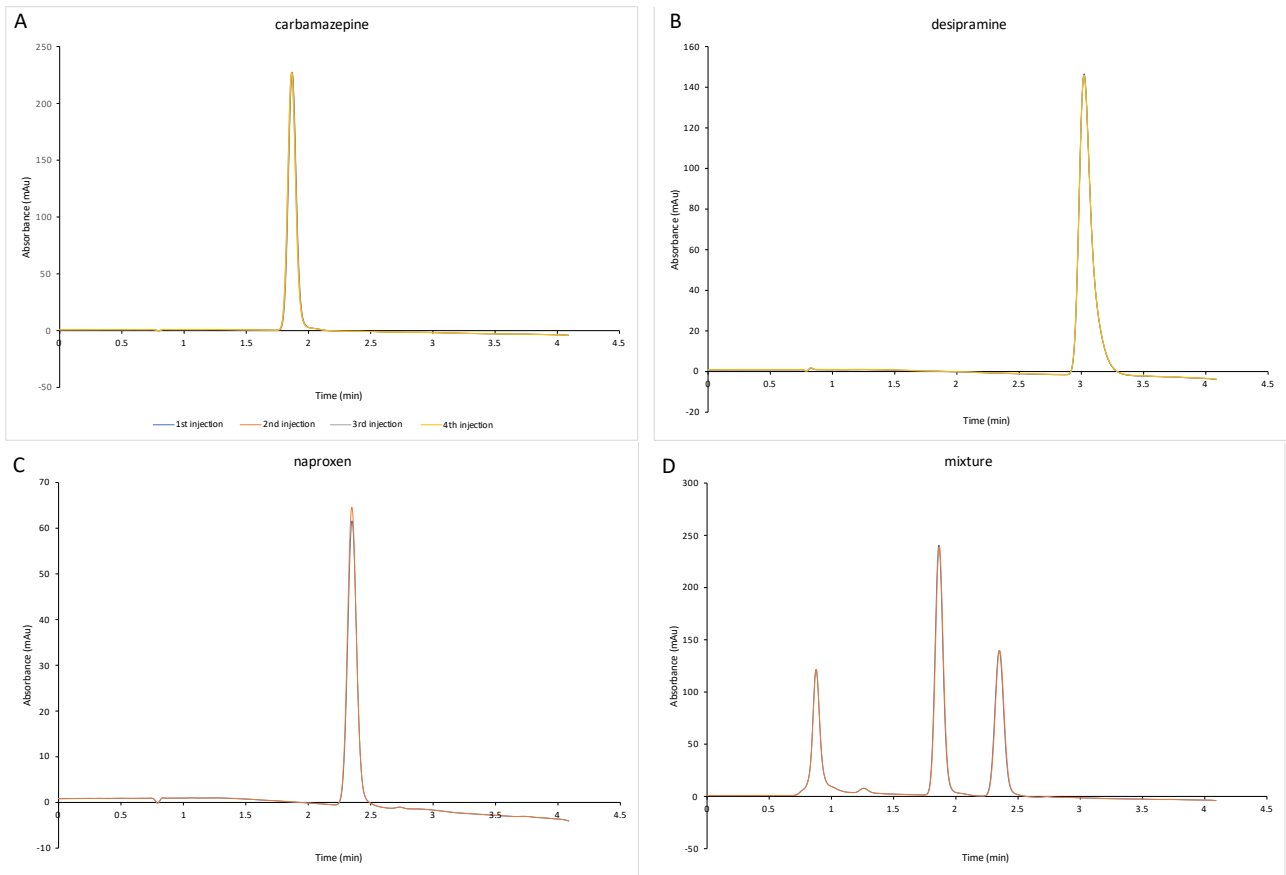
557

558

559

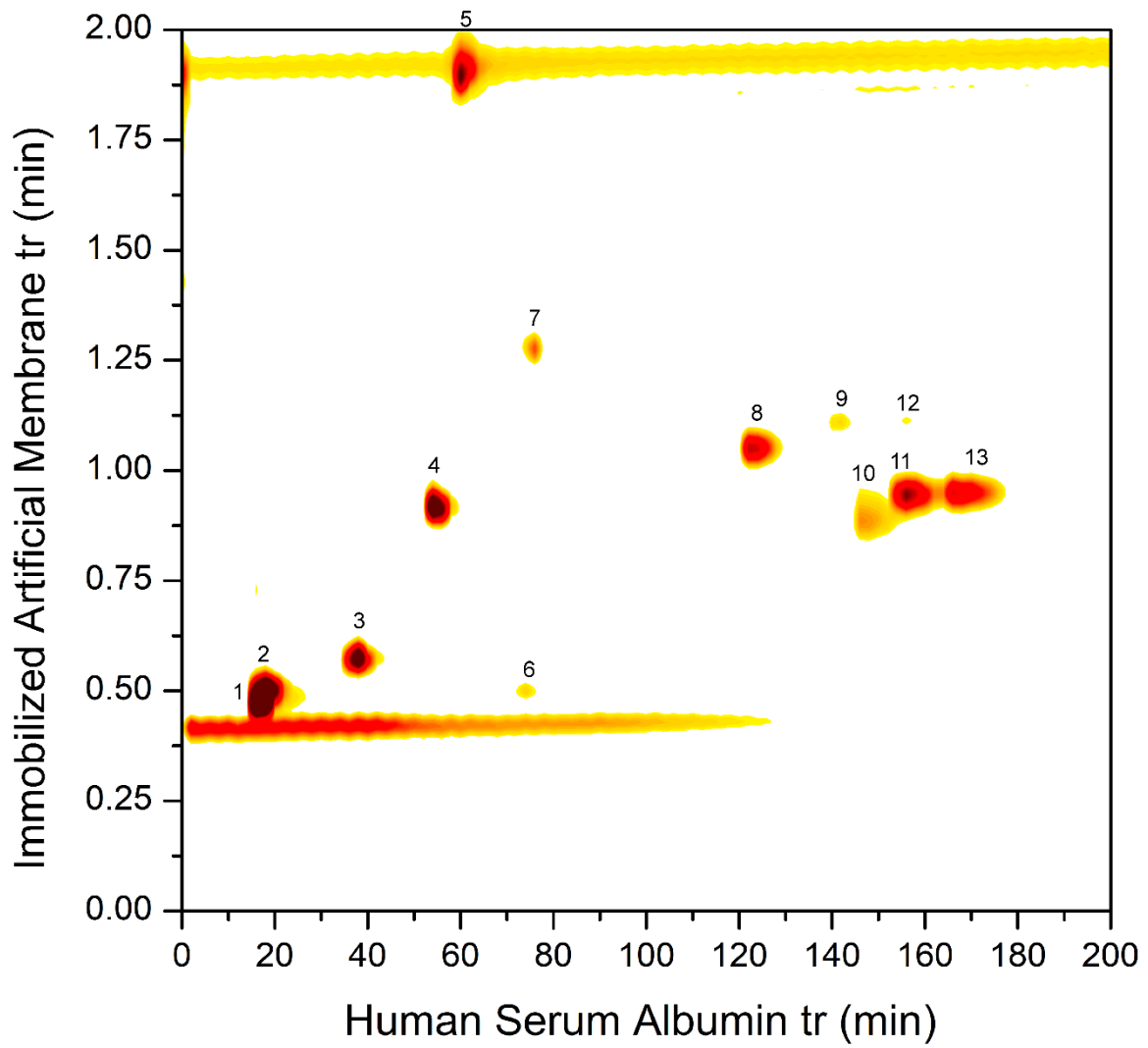
560

561 **Figure 1.**



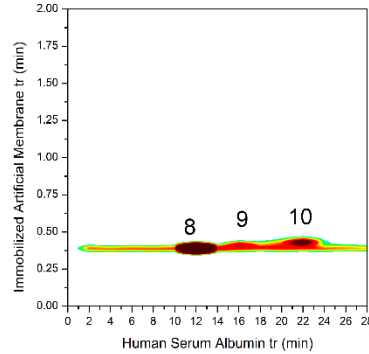
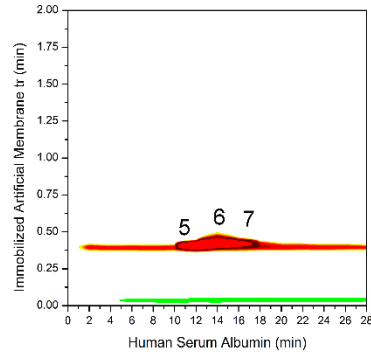
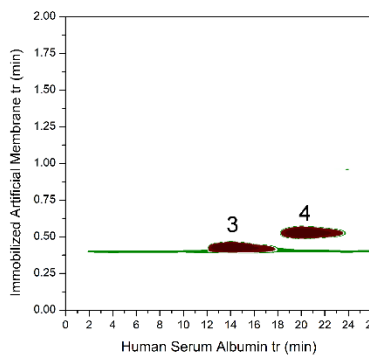
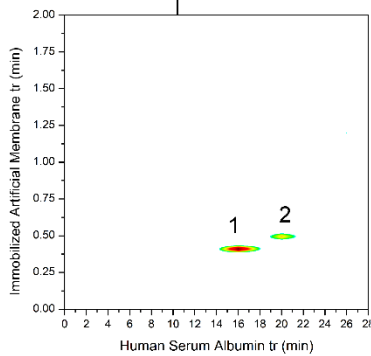
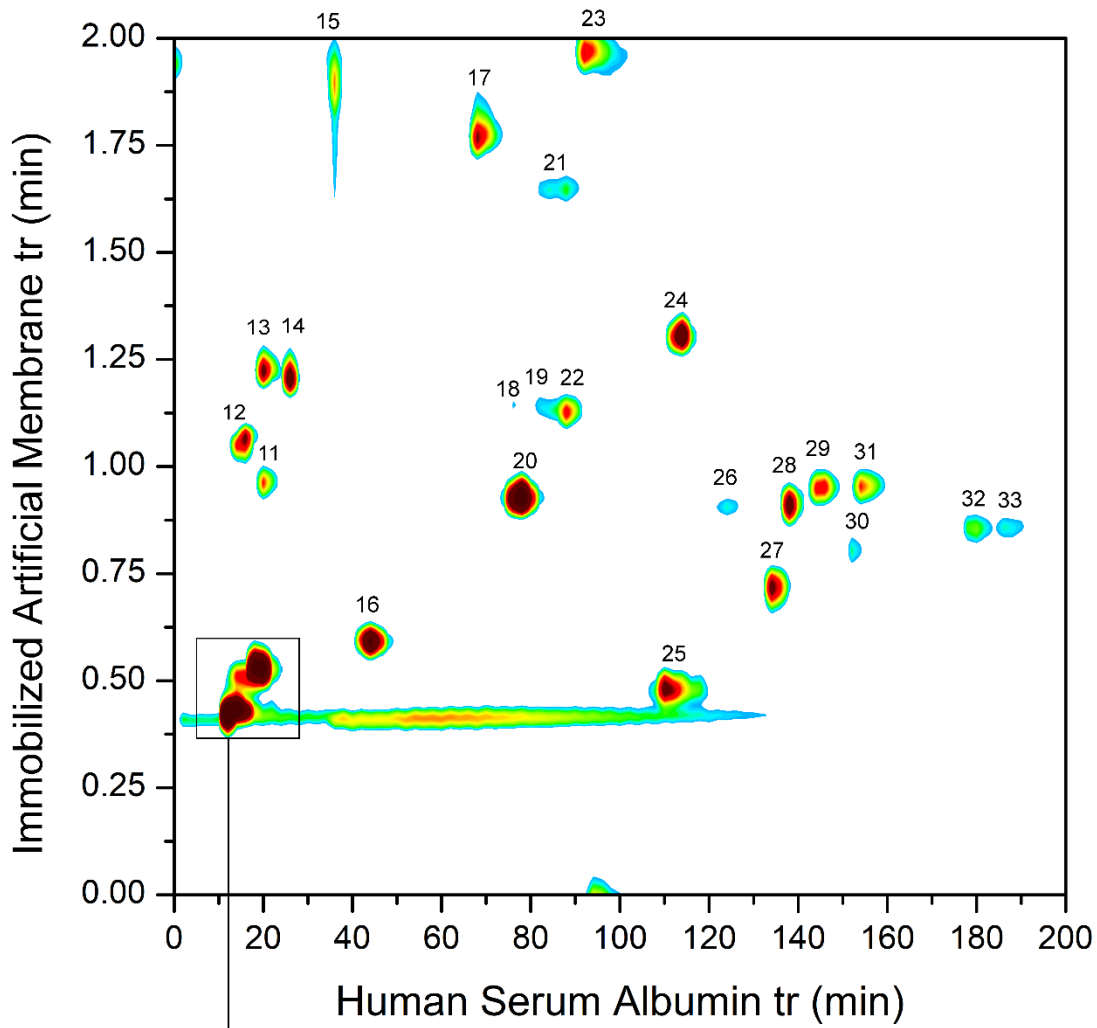
562
563
564
565
566
567
568
569
570
571
572
573
574
575
576
577
578
579
580
581
582
583
584
585
586

587 **Figure 2**



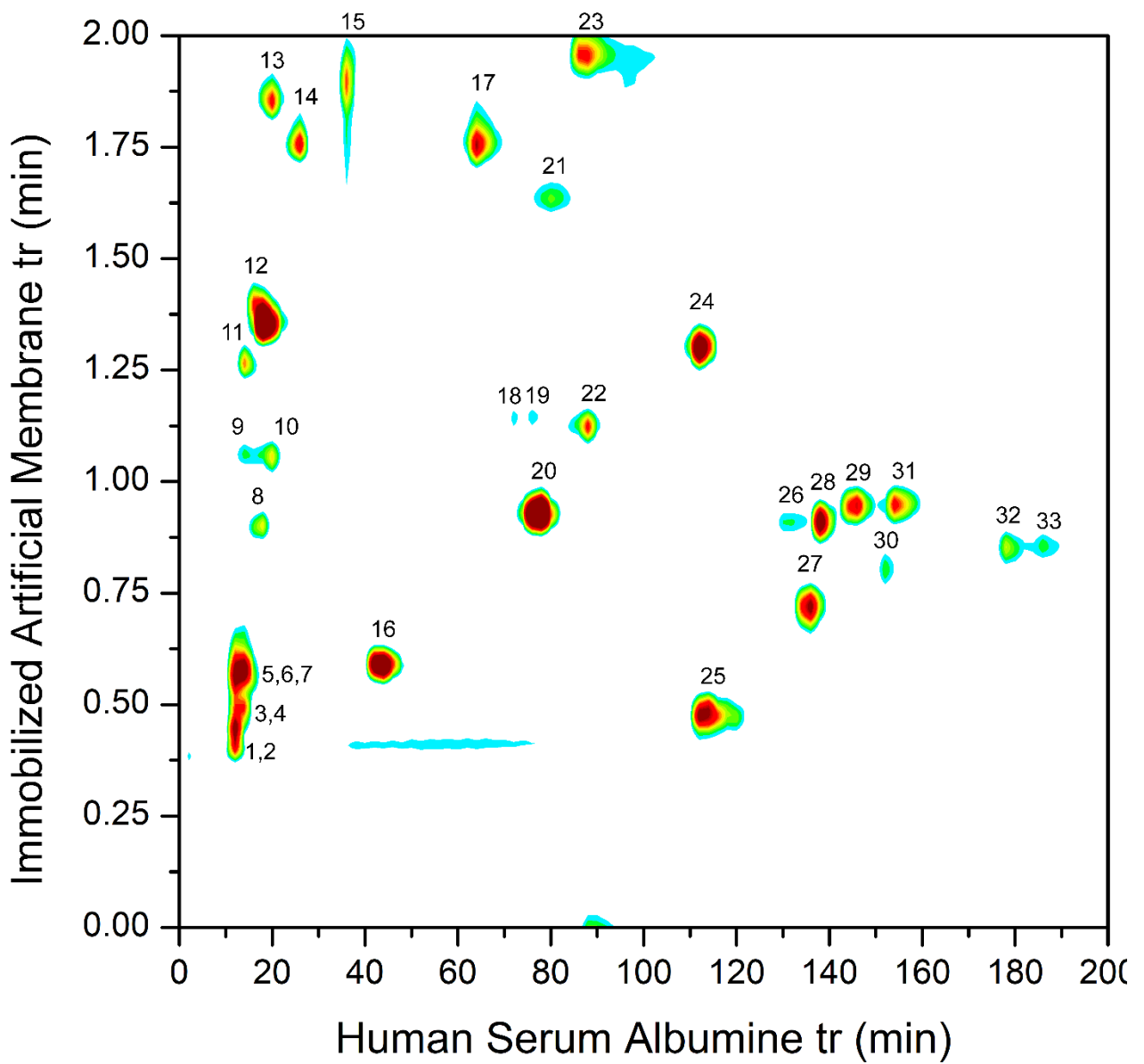
- | | | |
|------------------------|-------------------|--------------------|
| 1. acetaminophen | 6. salicylic acid | 11. (-)-ketoprofen |
| 2. antipyrine | 7. nifedipine | 12. (-)-warfarin |
| 3. hydrochlorothiazide | 8. losartan | 13. (+)-ketoprofen |
| 4. carbamazepine | 9. (+)-warfarin | |
| 5. desipramine | 10. piroxicam | |

588
589
590
591
592
593
594
595
596
597
598
599
600
601
602
603
604



- | | |
|-------------------------|----------------------|
| 1. acetaminophen | 21. nifedipine |
| 2. antipyrine | 22. (+)-griseofulvin |
| 3. lysinopril | 23. desipramine |
| 4. amiloride | 24. losartan |
| 5. enalaprilat | 25. salicylic acid |
| 6. L-phenylalanine | 26. (-)-fexofenadine |
| 7. creatinine | 27. furosemide |
| 8. valacyclovir | 28. (+)-fexofenadine |
| 9. enalapril | 29. (-)-fluvastatin |
| 10. terbutaline | 30. piroxicam |
| 11. cimetidine | 31. (+)-fluvastatin |
| 12. (±)-atenolol | 32. (-)-ketoprofen |
| 13. (±)-metoprolol | 33. (+)-ketoprofen |
| 14. ranitidine | |
| 15. cyclosporin A | |
| 16. hydrochlorothiazide | |
| 17. (±)-propranolol | |
| 18. (+)-verapamil | |
| 19. (-)-verapamil | |
| 20. carbamazepine | |

607 **Figure 4**



608

609

610

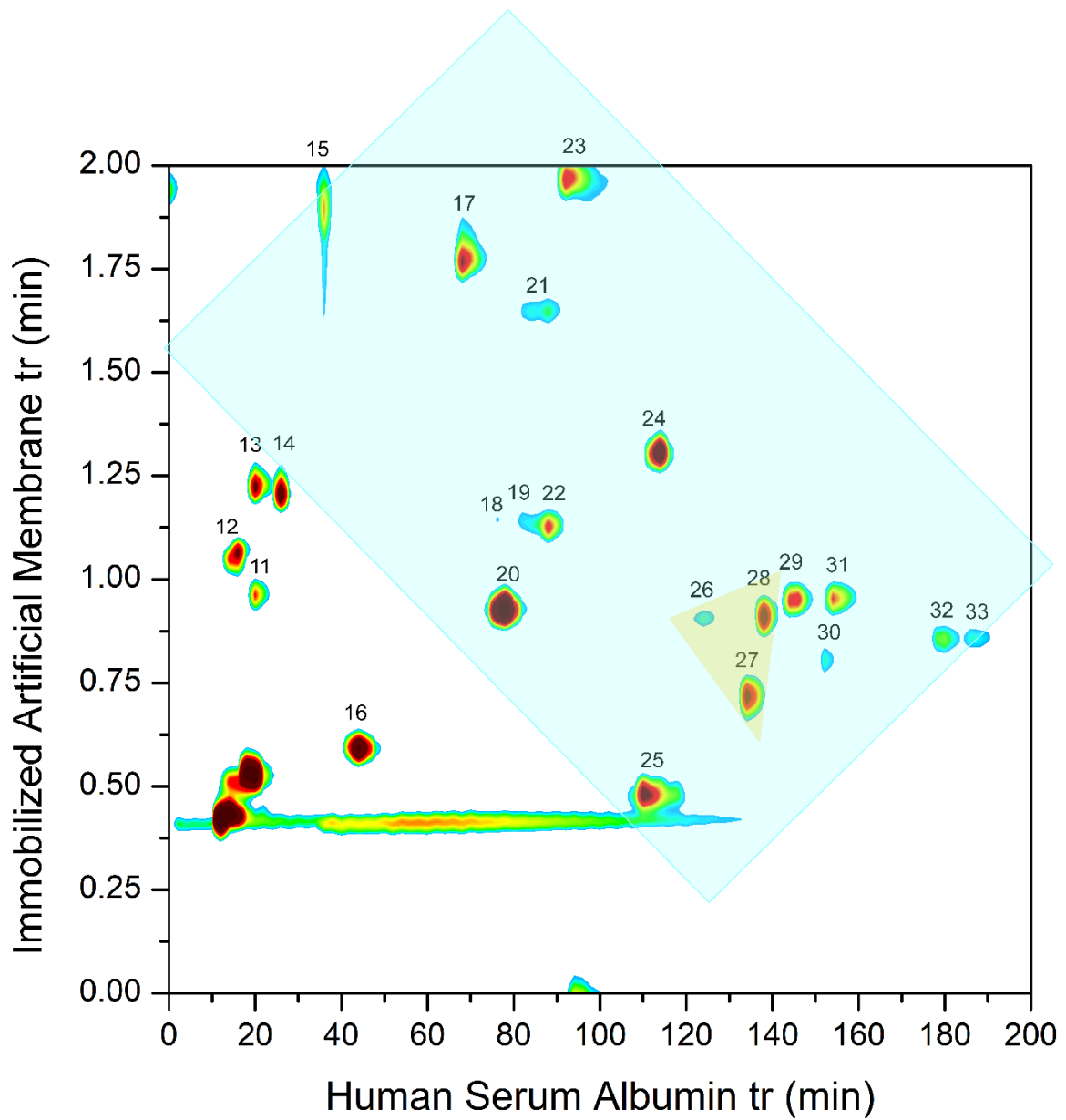
611

612

613

614

615



Intestinal effective permeability higher than $1.0 \times 10^{-4} \text{ cm} \cdot \text{sec}^{-1}$

Outliers

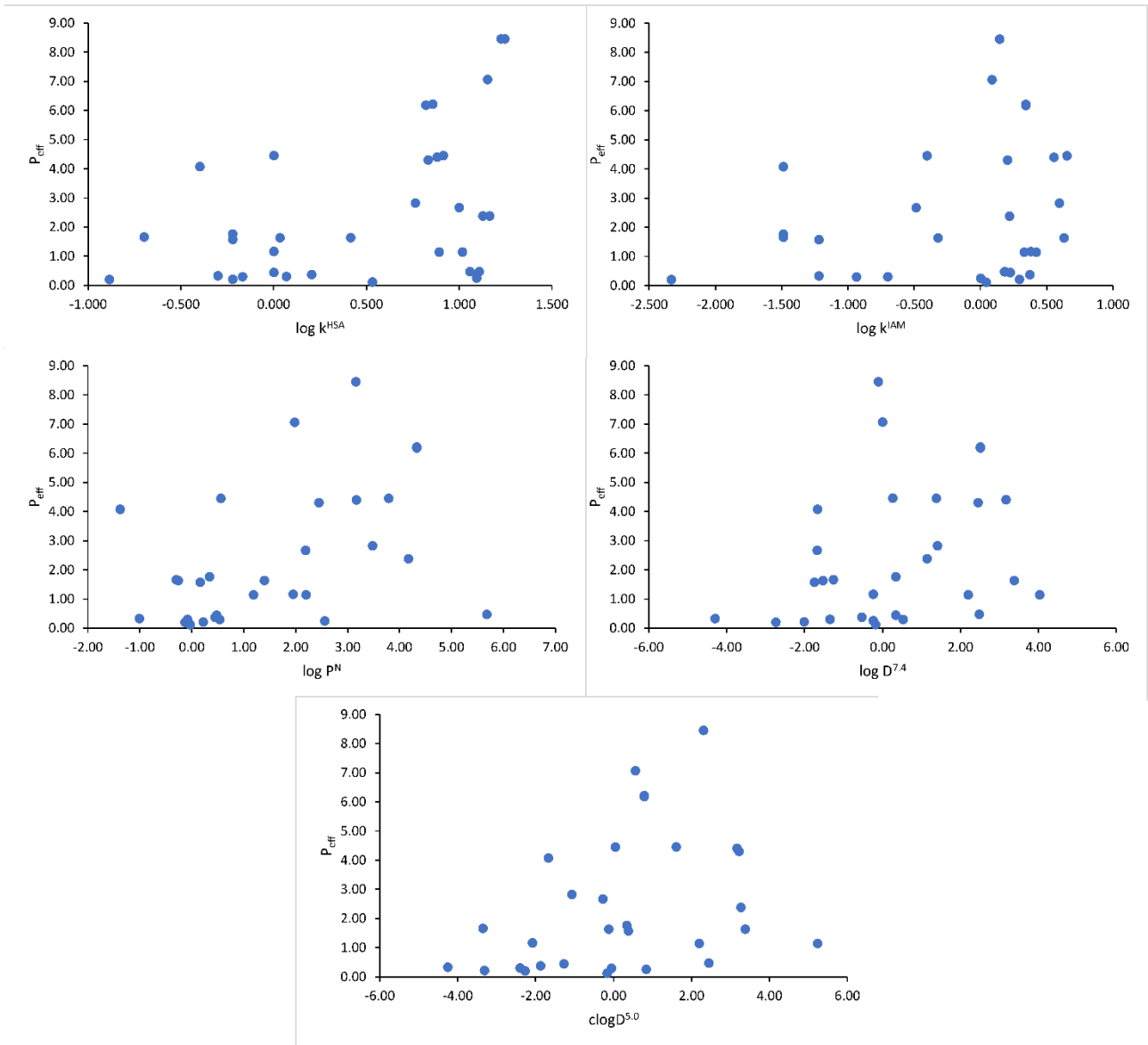
617

618

619

620

621 **Figure 6**



622

623

624

625

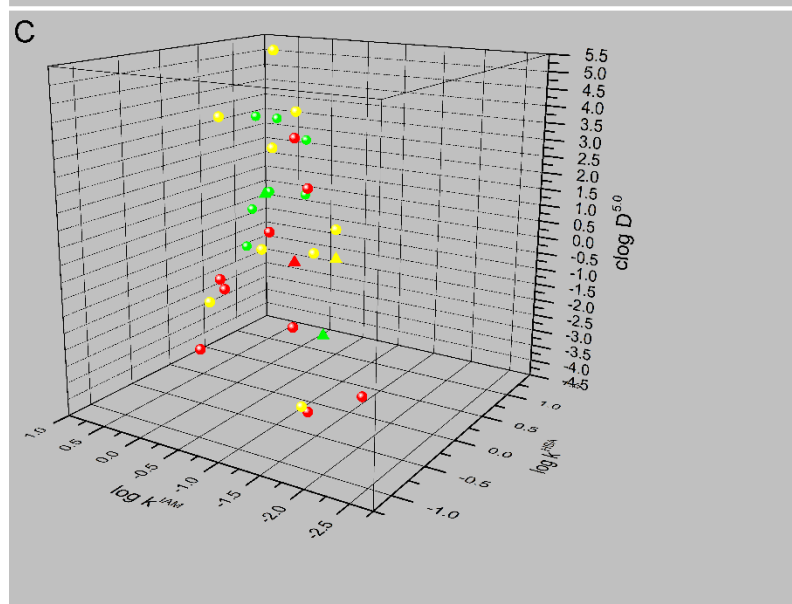
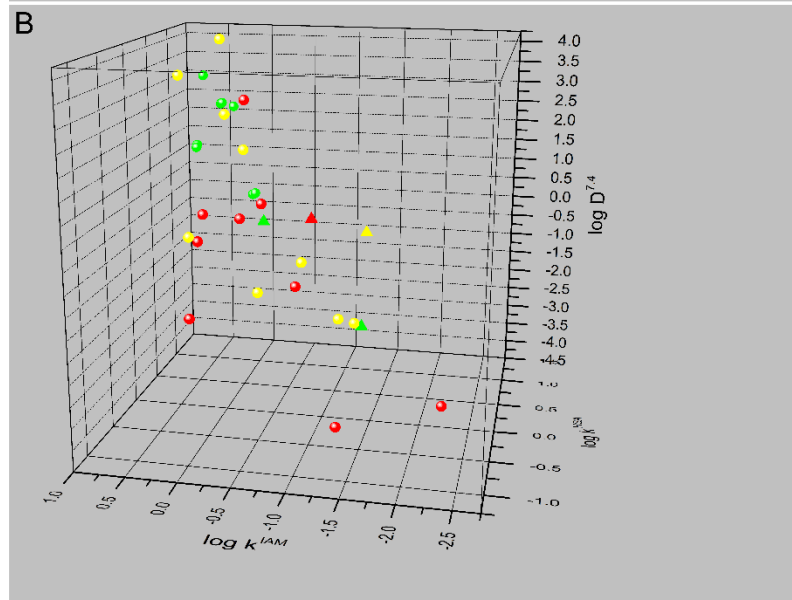
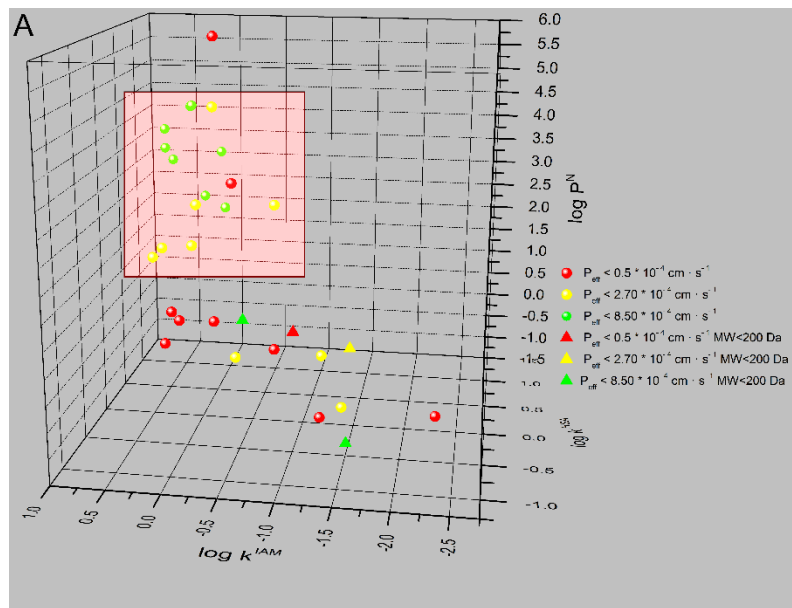
626

627

628

629

630



633 **Captions**

634

635 **Table 1.** Logarithms of chromatographic retention coefficients on the HSA ($\log k^{\text{HSA}}$) and IAM (\log
636 k^{IAM}) stationary phases, of the *n*-octanol/water partition coefficients of the neutral forms of the
637 analytes ($\log P^{\text{N}}$), of the distribution coefficients at 7.4 ($\log D^{7.4}$) and 5.0 ($\log D^{5.0}$) pH, intestinal
638 effective permeability values ($\times 10^{-4} \text{ cm} \cdot \text{s}^{-1}$) and supplier of the considered analytes.

639

640 **Figure 1.** IAM chromatograms showing four consecutive runs performed after flushing 20 column
641 volumes. A $25 \mu\text{g mL}^{-1}$ solution of the compounds carbamazepine (A), desipramine (B), naproxen
642 (C) and a mixture of acetaminophen, antipyrine, carbamazepine and naproxen (D) was injected.
643 Further details are reported in 2.0 of the supporting information.

644

645 **Figure 2.** Contour plot at 254 nm obtained for the HSA \times IAM separation of a test mixture for
646 competitive binding and HSA Site I occupancy assessment purposes. Further experimental details
647 are reported in 2.4 of the main body of the manuscript.

648

649 **Figure 3.** Contour plot at 220 nm obtained for the HSA \times IAM separation of a dataset for bioaffinity
650 measurements, in which the fixed gradient elution program is applied in ^2D for the whole duration
651 of the run. Further experimental details are reported in 2.5 of the main body of the manuscript.

652

653 **Figure 4.** Contour plot at 220 nm obtained for the HSA \times IAM separation of a dataset for bioaffinity
654 measurements, in which a segmented gradient elution program is applied in ^2D . Further
655 experimental details are reported in 2.5 of the main body of the manuscript.

656

657 **Figure 5.** Contour plot at 220 nm obtained for the HSA × IAM separation of a dataset for Bioaffinity
658 measurements, in which a mixed gradient elution program is applied in 2D. The region in which
659 compounds feature favourable intestinal effective permeability is represented in a blue square.
660 The outliers are instead displayed in a yellow triangle.

661

662 **Figure 6.** Scatterplots in which the intestinal effective permeability is studied vs the logarithms of
663 chromatographic retention coefficients on the HSA ($\log k^{\text{HSA}}$, top left), IAM ($\log k^{\text{IAM}}$, top right)
664 stationary phases, the *n*-octanol/water partition coefficients of the neutral forms of the analytes
665 ($\log P^{\text{N}}$, middle left), of the distribution coefficients at pH 7.4 ($\log D^{7.4}$, middle right) and 5.0 pH
666 ($\text{clog } D^{5.0}$, bottom).

667

668 **Figure 7.** 3D scatterplot studying both HSA and IAM affinities vs the *n*-octanol/water partition
669 coefficient of the neutral forms of the analytes ($\log P^{\text{N}}$), of the distribution coefficient at 7.4 (\log
670 $D^{7.4}$) and 5.0 ($\text{clog } D^{5.0}$) pH. Compounds with mass weight lower than 200 Da are pictured in
671 triangles, whereas those heavier than 200 Da are circle shaped. The colors of the datapoints refer
672 to a good (green), medium (yellow) and poor (red) extent of intestinal effective permeability.

673

674

675

676

677

678

679

680

681 **References**

- 682 [1] L. Allen, H.C. Ansel, *Ansel's pharmaceutical dosage forms and drug delivery systems*, Lippincott
683 Williams & Wilkins 2013.
- 684 [2] H. Lennernas, Human intestinal permeability, *J Pharm Sci*, 87 (1998) 403-410.
- 685 [3] D. Porat, A. Dahan, Active intestinal drug absorption and the solubility-permeability interplay,
686 *Int J Pharm*, 537 (2018) 84-93.
- 687 [4] G.L. Amidon, H. Lennernas, V.P. Shah, J.R. Crison, A theoretical basis for a biopharmaceutic
688 drug classification: the correlation of in vitro drug product dissolution and in vivo bioavailability,
689 *Pharm Res*, 12 (1995) 413-420.
- 690 [5] M. Lindenberg, S. Kopp, J.B. Dressman, Classification of orally administered drugs on the World
691 Health Organization Model list of Essential Medicines according to the biopharmaceutics
692 classification system, *Eur J Pharm Biopharm*, 58 (2004) 265-278.
- 693 [6] P. Stenberg, K. Luthman, P. Artursson, Virtual screening of intestinal drug permeability, *J*
694 *Control Release*, 65 (2000) 231-243.
- 695 [7] Z.G. Oner, J.E. Polli, Bioavailability and Bioequivalence, *ADME Processes in Pharmaceutical*
696 *Sciences*, Springer 2018, pp. 223-240.
- 697 [8] D. Dahlgren, C. Roos, E. Sjogren, H. Lennernas, Direct In Vivo Human Intestinal Permeability
698 (Peff) Determined with Different Clinical Perfusion and Intubation Methods, *J Pharm Sci*, 104
699 (2015) 2702-2726.
- 700 [9] K. Valko, S. Nunhuck, C. Bevan, M.H. Abraham, D.P. Reynolds, Fast gradient HPLC method to
701 determine compounds binding to human serum albumin. Relationships with octanol/water and
702 immobilized artificial membrane lipophilicity, *J Pharm Sci*, 92 (2003) 2236-2248.
- 703 [10] F. Hollosy, K. Valko, A. Hersey, S. Nunhuck, G. Keri, C. Bevan, Estimation of volume of
704 distribution in humans from high throughput HPLC-based measurements of human serum albumin
705 binding and immobilized artificial membrane partitioning, *J Med Chem*, 49 (2006) 6958-6971.
- 706 [11] Q. Hu, Y. Bu, R. Cao, G. Zhang, X. Xie, S. Wang, Stability Designs of Cell Membrane Cloaked
707 Magnetic Carbon Nanotubes for Improved Life Span in Screening Drug Leads, *Analytical chemistry*,
708 91 (2019) 13062-13070.
- 709 [12] Y. Bu, Q. Hu, X. Zhang, T. Li, X. Xie, S. Wang, A novel cell membrane-cloaked magnetic
710 nanogripper with enhanced stability for drug discovery, *Biomaterials Science*, 8 (2020) 673-681.
- 711 [13] L. Grumetto, F. Barbato, G. Russo, Scrutinizing the interactions between bisphenol analogues
712 and plasma proteins: Insights from biomimetic liquid chromatography, molecular docking
713 simulations and in silico predictions, *Environ Toxicol Pharmacol*, 68 (2019) 148-154.
- 714 [14] Y. Wang, S. Wang, M. Huang, Structure and enzymatic activities of human serum albumin,
715 *Curr Pharm Des*, 21 (2015) 1831-1836.
- 716 [15] D.G. Levitt, M.D. Levitt, Human serum albumin homeostasis: a new look at the roles of
717 synthesis, catabolism, renal and gastrointestinal excretion, and the clinical value of serum albumin
718 measurements, *Int J Gen Med*, 9 (2016) 229-255.
- 719 [16] C. Pidgeon, U.V. Venkataram, Immobilized artificial membrane chromatography: supports
720 composed of membrane lipids, *Anal Biochem*, 176 (1989) 36-47.
- 721 [17] C. Pidgeon, S. Ong, H. Liu, X. Qiu, M. Pidgeon, A.H. Dantzig, J. Munroe, W.J. Hornback, J.S.
722 Kasher, L. Glunz, et al., IAM chromatography: an in vitro screen for predicting drug membrane
723 permeability, *J Med Chem*, 38 (1995) 590-594.
- 724 [18] L. Grumetto, G. Russo, F. Barbato, Indexes of polar interactions between ionizable drugs and
725 membrane phospholipids measured by IAM-HPLC: their relationships with data of Blood-Brain
726 Barrier passage, *Eur J Pharm Sci*, 65 (2014) 139-146.

727 [19] L. Grumetto, G. Russo, F. Barbato, Relationships between human intestinal absorption and
728 polar interactions drug/phospholipids estimated by IAM-HPLC, *Int J Pharm*, 489 (2015) 186-194.

729 [20] L. Grumetto, G. Russo, F. Barbato, Immobilized Artificial Membrane HPLC Derived Parameters
730 vs PAMPA-BBB Data in Estimating in Situ Measured Blood-Brain Barrier Permeation of Drugs, *Mol*
731 *Pharm*, 13 (2016) 2808-2816.

732 [21] L. Grumetto, G. Russo, F. Barbato, Polar interactions drug/phospholipids estimated by IAM-
733 HPLC vs cultured cell line passage data: Their relationships and comparison of their effectiveness
734 in predicting drug human intestinal absorption, *Int J Pharm*, 500 (2016) 275-290.

735 [22] G. Russo, L. Grumetto, R. Szucs, F. Barbato, F. Lynen, Determination of in Vitro and in Silico
736 Indexes for the Modeling of Blood-Brain Barrier Partitioning of Drugs via Micellar and Immobilized
737 Artificial Membrane Liquid Chromatography, *J Med Chem*, 60 (2017) 3739-3754.

738 [23] G. Russo, L. Grumetto, R. Szucs, F. Barbato, F. Lynen, Screening therapeutics according to their
739 uptake across the blood-brain barrier: A high throughput method based on immobilized artificial
740 membrane liquid chromatography-diode-array-detection coupled to electrospray-time-of-flight
741 mass spectrometry, *Eur J Pharm Biopharm*, (2018).

742 [24] F. Tsopeles, T. Vallianatou, A. Tsantili-Kakoulidou, Advances in immobilized artificial
743 membrane (IAM) chromatography for novel drug discovery, *Expert Opinion on Drug Discovery*, 11
744 (2016) 473-488.

745 [25] J. Kotecha, S. Shah, I. Rathod, G. Subbaiah, Prediction of oral absorption in humans by
746 experimental immobilized artificial membrane chromatography indices and physicochemical
747 descriptors, *International Journal of Pharmaceutics*, 360 (2008) 96-106.

748 [26] D. Guillarme, J. Ruta, S. Rudaz, J.L. Veuthey, New trends in fast and high-resolution liquid
749 chromatography: a critical comparison of existing approaches, *Anal Bioanal Chem*, 397 (2010)
750 1069-1082.

751 [27] B.W.J. Pirok, A.F.G. Gargano, P.J. Schoenmakers, Optimizing separations in online
752 comprehensive two-dimensional liquid chromatography, *J Sep Sci*, 41 (2018) 68-98.

753 [28] A. Avdeef, Octanol–water partitioning, in: J.W. Sons (Ed.) *Absorption and Drug Development*
754 Hoboken, NJ, USA 2012, pp. 201-209.

755 [29] D.S. Wishart, Y.D. Feunang, A.C. Guo, E.J. Lo, A. Marcu, J.R. Grant, T. Sajed, D. Johnson, C. Li, Z.
756 Sayeeda, N. Assempour, I. Iynkkaran, Y. Liu, A. Maciejewski, N. Gale, A. Wilson, L. Chin, R.
757 Cummings, D. Le, A. Pon, C. Knox, M. Wilson, DrugBank 5.0: a major update to the DrugBank
758 database for 2018, *Nucleic Acids Res*, 46 (2018) D1074-D1082.

759 [30] M.S.f.W.-b.P.v. <http://www.chemaxon.com/products/marvin/marvinsketch/>, Calculation
760 module designed by Chemaxon.

761 [31] A. Avdeef, Permeability: Caco-2/MDCK, in: J.W. Sons (Ed.) *Absorption and Drug Development*
762 Hoboken, NJ, USA 2012, pp. 539-541.

763 [32] E. Sjogren, D. Dahlgren, C. Roos, H. Lennernas, Human in vivo regional intestinal permeability:
764 quantitation using site-specific drug absorption data, *Mol Pharm*, 12 (2015) 2026-2039.

765 [33] C.T.I. Daicel group, INSTRUCTION MANUAL FOR CHIRALPAK® HSA, 2013.

766 [34] P.C. Acharya, C. Fernandes, S. Mallik, B. Mishra, R.K. Tekade, Chapter 4 - Physiologic Factors
767 Related to Drug Absorption, in: R.K. Tekade (Ed.) *Dosage Form Design Considerations*, Academic
768 Press 2018, pp. 117-147.

769 [35] A. Avdeef, K.J. Box, J.E. Comer, C. Hibbert, K.Y. Tam, pH-metric logP 10. Determination of
770 liposomal membrane-water partition coefficients of ionizable drugs, *Pharm Res*, 15 (1998) 209-
771 215.

772 [36] M. Gilar, P. Olivova, A.E. Daly, J.C. Gebler, Orthogonality of separation in two-dimensional
773 liquid chromatography, *Anal Chem*, 77 (2005) 6426-6434.

774 [37] D.V. McCalley, A study of column equilibration time in hydrophilic interaction
775 chromatography, *J Chromatogr A*, 1554 (2018) 61-70.

776 [38] P. Venter, M. Muller, J. Vestner, M.A. Stander, A.G.J. Tredoux, H. Pasch, A. de Villiers,
777 Comprehensive Three-Dimensional LC x LC x Ion Mobility Spectrometry Separation Combined with
778 High-Resolution MS for the Analysis of Complex Samples, *Anal Chem*, 90 (2018) 11643-11650.

779 [39] E. Domenici, C. Bertucci, P. Salvadori, G. Félix, I. Cahagne, S. Motellier, I.W. Wainer, Synthesis
780 and chromatographic properties of an HPLC chiral stationary phase based upon human serum
781 albumin, *Chromatographia*, 29 (1990) 170-176.

782 [40] G.A. Ascoli, C. Bertucci, P. Salvadori, Ligand binding to a human serum albumin stationary
783 phase: use of same-drug competition to discriminate pharmacologically relevant interactions,
784 *Biomed Chromatogr*, 12 (1998) 248-254.

785 [41] G.A. Ascoli, E. Domenici, C. Bertucci, Drug binding to human serum albumin: abridged review
786 of results obtained with high-performance liquid chromatography and circular dichroism, *Chirality*,
787 18 (2006) 667-679.

788 [42] H. Zou, H. Wang, Y. Zhang, Stereoselective Binding of Warfarin and Ketoprofen to Human
789 Serum Albumin Determined by Microdialysis Combined with HPLC, *Journal of Liquid*
790 *Chromatography & Related Technologies*, 21 (1998) 2663-2674.

791 [43] G. Russo, L. Grumetto, F. Barbato, G. Vistoli, A. Pedretti, Prediction and mechanism
792 elucidation of analyte retention on phospholipid stationary phases (IAM-HPLC) by in silico
793 calculated physico-chemical descriptors, *Eur J Pharm Sci*, 99 (2017) 173-184.

794 [44] G. Colmenarejo, In silico prediction of drug-binding strengths to human serum albumin,
795 *Medicinal Research Reviews*, 23 (2003) 275-301.

796 [45] S. Kim, J. Chen, T. Cheng, A. Gindulyte, J. He, S. He, Q. Li, B.A. Shoemaker, P.A. Thiessen, B. Yu,
797 L. Zaslavsky, J. Zhang, E.E. Bolton, PubChem 2019 update: improved access to chemical data,
798 *Nucleic Acids Research*, 47 (2018) D1102-D1109.

799 [46] C.D. Scripture, J.A. Pieper, Clinical Pharmacokinetics of Fluvastatin, *Clinical Pharmacokinetics*,
800 40 (2001) 263-281.

801 [47] F.L. Tse, D.F. Nickerson, W.S. Yardley, Binding of fluvastatin to blood cells and plasma
802 proteins, *J Pharm Sci*, 82 (1993) 942-947.

803 [48] L.N. Jattinagoudar, S.T. Nandibewoor, S.A. Chimatadar, Binding of fexofenadine hydrochloride
804 to bovine serum albumin: structural considerations by spectroscopic techniques and molecular
805 docking, *J Biomol Struct Dyn*, 35 (2017) 1200-1214.

806 [49] A. Samanta, S. Jana, D. Ray, N. Guchhait, Modulated photophysics of a cationic DNA-staining
807 dye inside protein bovine serum albumin: study of binding interaction and structural changes of
808 protein, *Spectrochim Acta A Mol Biomol Spectrosc*, 121 (2014) 23-34.

809 [50] S.D. Flanagan, L.H. Takahashi, X. Liu, L.Z. Benet, Contributions of saturable active secretion,
810 passive transcellular, and paracellular diffusion to the overall transport of furosemide across
811 adenocarcinoma (Caco-2) cells, *J Pharm Sci*, 91 (2002) 1169-1177.

812 [51] N. Petri, C. Tannergren, D. Rungstad, H. Lennernas, Transport characteristics of fexofenadine
813 in the Caco-2 cell model, *Pharm Res*, 21 (2004) 1398-1404.

814 [52] B. Pecoraro, M. Tutone, E. Hoffman, V. Hutter, A.M. Almerico, M. Traynor, Predicting Skin
815 Permeability by Means of Computational Approaches: Reliability and Caveats in Pharmaceutical
816 Studies, *J Chem Inf Model*, 59 (2019) 1759-1771.

817 [53] C. Giaginis, A. Tsantili-Kakoulidou, Current State of the Art in HPLC Methodology for
818 Lipophilicity Assessment of Basic Drugs. A Review, *Journal of Liquid Chromatography & Related*
819 *Technologies*, 31 (2007) 79-96.

820 [54] S.C. Pearce, A. Al-Jawadi, K. Kishida, S. Yu, M. Hu, L.F. Fritzy, K.L. Edelblum, N. Gao, R.P.
821 Ferraris, Marked differences in tight junction composition and macromolecular permeability
822 among different intestinal cell types, *BMC Biol*, 16 (2018) 19.
823 [55] P.D. Leeson, B. Springthorpe, The influence of drug-like concepts on decision-making in
824 medicinal chemistry, *Nature Reviews Drug Discovery*, 6 (2007) 881-890.
825